Journal of Nuclear Materials 434 (2013) 1–6

Contents lists available at SciVerse ScienceDirect

Journal of Nuclear Materials

journal homepage: www.elsevier.com/locate/jnucmat

Molecular dynamics simulation of deuterium trapping and bubble formation in tungsten

Xue Yang *, Ahmed Hassanein

Center for Material under Extreme Environment, School of Nuclear Engineering, Purdue University, West Lafayette, IN 47907, USA

HIGHLIGHTS

- Deuterium tungsten interaction was simulated using classical molecular dynamic methods.
- Low energy deuterium atoms tend to affix to high temperature tungsten surface.
- Tungsten substrate temperature barely affects the low energy deuterium implantation depth.
- Deuterium bubble formation resulting from near surface super-saturation was predicted.

ARTICLE INFO

Article history:
Received 18 May 2012
Accepted 30 October 2012
Available online 15 November 2012

ABSTRACT

The interaction between plasma particles and tungsten as plasma facing material is one of the critical issues in successfully using tungsten in Tokamak reactors environment. The deuterium bombardment of monocrystalline tungsten was modeled by molecular dynamics simulation using LAMMPS code and Tersoff type interatomic potential. The deuterium trapping rate, implantation depth, and the stopping time in tungsten at several temperatures ranging from 600 to 2000 K bombarded by 5–100 eV deuterium atoms were simulated. Deuterium bubble formation at near tungsten surface was also studied. Irradiated monocrystalline tungsten became amorphous state prior to deuterium cluster formation, and gas bubbles were observed in the 600, 900, and 1200 K tungsten samples. The formation of gas bubbles were caused by the near surface deuterium super-saturation region and the subsequent plastic deformation induced by the local high gas pressure.

Published by Elsevier B.V.

1. Introduction

Tungsten as a potential candidate for plasma facing materials (PFMs) in Tokomaks has several distinct advantages. Tungsten has a very high melting point (3400 °C), conducts heat away efficiently, and can withstand high plasma particle and heat fluxes. Because hydrogen usually does not chemically bond with tungsten atom, there is no chemical sputtering when bombarded by hydrogen isotope ions. This results in very low overall tungsten erosion rate [1]. In addition, tungsten is a high Z material, therefore the physical sputtering yield is low, and requires incident ion with higher energy to cause significant sputtering (e.g. sputtering rate 10^{-4} for 250 eV deuterium ions [1]). Therefore, tungsten dust generation during the operation is assumed much lower than other PFM such as carbon fiber composites (CFCs) and Be. However, hydrogen atoms are highly mobile in tungsten, and they tend to be trapped at the crystallographic defect sites to form cluster, bubble, or blister [2,3]. The burst of blisters may eject tungsten dust and macroscopic particles into the plasma [4]. Because high Z dust and debris will quench the plasma energy and cause plasma collapse/disruption, hydrogen retention and bubble formation are critical issues in using tungsten as PFM and such effects are still not well understood.

The classic molecular dynamic (MD) simulation is a numerical simulation tool of physical movements of atoms and molecules whose trajectories are determined by Newton's equation of motion. The MD simulation has been used for investigating various phenomena in the field of plasma material interaction. Helium cluster, bubble, or blister formation processes on tungsten surface [5–7] or liquid lithium [8] has been recently studied, while others investigated the low energy (~100 eV) deuterium implantation on tungsten carbide with or without impurities (i.e., C, W, He, Ne, or Ar, etc.) [8–12]. More recent work [13–19] has been done in studying various impact of tungsten bombarded by hydrogen and deuterium. In this work we use MD simulation to model the trapping of deuterium in tungsten and as a result, conditions of bubble formation. The deuterium retention rate, implantation depth, and stopping time were calculated. Possible mechanisms of deuterium bubble formation at tungsten surface were also discussed.

* Corresponding author. Tel.: +1 7654049997.
E-mail address: yang99@purdue.edu (X. Yang).

0022-3115/$ - see front matter Published by Elsevier B.V.
http://dx.doi.org/10.1016/j.jnucmat.2012.10.045

2. Simulation method and configuration

2.1. Interatomic potential

The classical molecular dynamic LAMMPS code [20] was used in this simulation to study the deuterium–tungsten interactions. Determining an appropriate W–H interatomic potential is very important in this MD simulation. In the past, the simple pair potentials were usually used, such as the Morse potential [21,22] and the universal force field potential [23]. Recently, with the increasing speed of computers, empirical (analytical) many-body potential, such as Analytic Bond-Order Potential (ABOP) became popular. These potentials describe atom-binding states, and therefore are able to describe the chemical bonding reactions with reasonable accuracy. Among the available ABOP potentials with sufficient data are the W–C–H potential [24] and W–H potential [25]. Kurtz [26] compared two ABOP potentials (mainly the W–W interaction) and shows that W–C–H potential developed by Juslin produces less accurate point defect properties and underestimates tungsten melting point. The W–H potential developed by Li has long cutoff parameter that requires 3–4 times longer runtime, and it overestimates the tungsten melting point. The W–H potential parameters may not be correct, because the interstitial properties did not reproduce Li's values. To be consistent with the subsequent C and H mixture bombardment modeling, the W–C–H ABOP developed by Juslin was chosen as the interatomic potential to describe the interaction between tungsten and deuterium ions.

There is no direct ABOP implementation in LAMMPS, but the ABOP formula can be transformed to the Tersoff implementation in LAMMPS using the following formulation:

$$\begin{aligned}
&m^{LAM} = n^{LAM} = 1\\
&\beta^{LAM} = \omega\\
&\lambda_1^{LAM} = \beta\sqrt{2S}\\
&\lambda_2^{LAM} = \beta\sqrt{\tfrac{2}{S}}\\
&\lambda_3^{LAM} = \alpha_{ijk}\\
&(\cos\theta_0)^{LAM} = -h\\
&A^{LAM} = \tfrac{D_0}{S-1}e^{\lambda_1^{LAM} r_0}\\
&B^{LAM} = \tfrac{SD_0}{S-1}e^{\lambda_2^{LAM} r_0}\\
&R^{LAM},\ D^{LAM},\ c^{LAM},\ d^{LAM},\ \gamma^{LAM} = R,\ D,\ c,\ d,\ \gamma
\end{aligned} \tag{1}$$

where the letters with *LAM* superscript denotes the LAMMPS Tersoff potential variables, while the others are the ABOP coefficients from Ref. [24]. For a Tersoff potential that models three-body interaction *ijk*, where the first element *i* is the center atom in the three-body interactions which is bonded to the second atom *j* and their bond is influenced by the third atom *k*, the n, β, λ_1, λ_2, A and B are used for the two-body interactions, while the R and D parameters are used for both two- and three-body interactions. The rest are used in the three-body interactions. The parameters used for two-body interaction that is converted from Ref. [24] according to Eq. (1) are obtained from the entry where the second element is repeated. For example, the two-body parameters of WHH entry in LAMMPS will use the WH parameters converted from Ref. [24]. Using the symmetric mixing rules, the two-body parameters of HWW are identical to the WHH parameters. The parameters used for two-body interactions in entries whose second and third element are different, such as WHW, are not used and can be set to zero. Therefore, a LAMMPS Tersoff potential file containing 27 entries describing the WCH ternary system is constructed. To validate the converted Tersoff potential, the cohesive energy, lattice parameter of the body-centered cubic tungsten; bond length, H–W–H bond angle and cohesive energy of the WH_x molecule are calculated using LAMMPS and the results match the reference data well [24].

2.2. Simulation configuration

The crystal structure of the tungsten sample used in this simulation is body-centered cubic (bcc) with a size of 8 by 5 by 55 lattices. A lattice parameter of 3.165 Å was used to construct the tungsten sample, because it yields the minimum potential energy based on the bcc tungsten energy minimization calculation. The top and bottom boundary conditions are non-periodic and fixed (particles do not interact across the boundary and do not move from one side of the box to the other; if an atom moves outside the boundary it will be removed from the system), while all other sides are set to be periodic. The bottom three layers of tungsten atoms are fixed in the space: the force on those atoms is zeroed out and the initial velocity of those atoms is zero. Prior to the bombardment, the mobile tungsten atoms are assigned an initial velocity based on the desired tungsten temperature with a Gaussian distribution. Then, the temperature rescaling is performed for 1000 steps using 0.01 ps as step size. During the bombardment, two layers of the tungsten atoms above the fixed atoms and one layer surrounding the side of the tungsten bulk is maintained at the desired temperature using Berendsen thermostat. The temperature is set to relax in a time span of 0.01 ps.

3. Simulation results and discussion

3.1. Deuterium trapping

To investigate the deuterium retention on tungsten sample, the following non-accumulative bombardment simulation procedure was performed for various tungsten temperatures and deuterium energies. During the deuterium bombardment, each deuterium atom was randomly placed two lattice parameters (6.33 Å) above the tungsten sample and then directed toward the surface with the specified energy. The step size during the bombardment was set to 0.5 fs. For every 100 steps, we check if the deuterium atom energy is lower than 0.5 eV or the deuterium atom escapes from the upper simulation box boundary. If the deuterium energy is lower than 0.5 eV, the deuterium atom barely moves and it can be considered as an interstitial atom in the tungsten sample, and the final deuterium location is recorded. The interstitial deuterium is then deleted and a new deuterium atom is initiated. When the incoming deuterium energy is slowed down to below 0.5 eV, the system temperature is very close to the desired temperature, and the low energy deuterium cannot displace tungsten atom (displacement threshold: 940 eV [27]). The 5–100 eV deuterium bombardment on tungsten does not cause any direct atomic displacement. Therefore, the tungsten substrate does not require re-equilibration, and it is ready for reuse right after the deletion of the interstitial deuterium atom. If the deuterium travels outside the simulation box boundaries, the deuterium atom is instantly deleted and the next deuterium will be directed towards the sample. The total number of deuterium atoms created for each run is 5000. The current simulation impinges deuterium atoms into 600, 1200, 1500, 1800 and 2000 K tungsten samples. The deuterium atom energies are between 5 and 100 eV, and the incident angle is 25° for all the simulations.

3.1.1. Deuterium retention rate on tungsten

The deuterium retention rate is defined as the total number of deuterium trapped in tungsten divided by the total number of deuterium incident into the tungsten (5000 atoms). All other incident ions either are directly reflected back at the surface or are bounced

in the sample and then escape from the surface before completely stop. Fig. 1a shows the deuterium retention rate for various deuterium energies and substrate temperatures. For higher deuterium energies, the retention rate is almost the same for different tungsten temperatures. For lower tungsten temperatures (<1500 K), the retention rate exhibits an increasing trend as function of the deuterium energy, because higher deuterium energy has higher probability to penetrate the tungsten surface instead of being reflected back or migrating to and escaping from the sample surface. For higher tungsten temperatures (>1800 K), the retention rate of low deuterium energy is much higher than the retention rate of the low tungsten temperatures.

To investigate this effect, the atomic deuterium sticking coefficients were calculated. The deuterium atom was considered to be stuck on the surface (absorbed) if the z coordinate of the final deuterium position is above -3.165 Å. This condition means that the absorbed D atoms were required to be within one lattice parameter of the surface. The sticking coefficient S is defined here as the number of D atoms stuck on the surface divided by the total incident deuterium atoms. The sticking coefficients were plotted in Fig. 1b. It shows that for higher incident deuterium energy, the sticking coefficients are very low indicating that almost all trapped deuterium atoms penetrate the tungsten surface. For the lower energy deuterium, the sticking coefficient is relatively large which results in higher retention rate for lower energy deuterium. Henriksson et al. used MD simulation with the same interatomic potential to calculate the sticking coefficients of deuterium with kinetic energies in the range of 0.003–10 eV on 300 K tungsten [19]. Similar trend was observed, i.e., incident deuterium with lower energy has higher sticking coefficient. The sticking coefficient of 5 and 10 eV deuterium on 300 K tungsten is about 0.03, which also match the trend that lower tungsten temperature tends to have lower sticking coefficient. The reason is assumed to be the relatively soft surface of the high temperature tungsten, which may serves as a cushion that helps the deuterium atom land on the surface. If the deuterium energy is high, this effect becomes insignificant and the retention rate is dominated by the longer penetration depth. It should be noted that the calculated retention rate is not based on the accumulative bombardment. For the real case, the trapped deuterium atom may migrate towards the surface due to the diffusion or thermal motion. It may also be accelerated by the subsequent atom impinging from cumulative bombardment, and knocked out from the substrate. In addition, deuterium atoms at the surface may form D_2 molecules and leave the surface. Therefore, the final deuterium retention rate could be much lower than calculated, especially at elevated temperature [28].

3.1.2. Deuterium implantation profile

If the kinetic energy of the deuterium atoms is lower than 0.5 eV and the deuterium atoms are inside the tungsten sample, the final position of such atoms is recorded. The average final depth of such atoms is plotted in Fig. 2. Based on these simulations, the tungsten temperature barely affects the average implantation depth which is almost proportional to the deuterium energy. For the case of 5 eV deuterium bombardments almost all retained deuterium atoms are on the surface. The W–H weak bond prevents the deuterium on the surface from leaving. Substrate temperature primarily affects the retention rate by affecting the reflection rate (probability that the incoming deuterium will be reflected back when the deuterium first contacts the tungsten surface). Temperature also affects surface recombination rate of D, which is not taken into account in this study [29]. Fig. 2 only reflects the initial resting positions of the implanted deuterium. In the cumulative bombardment, the embedded deuterium may shift due to the collision with the accumulated bombardment and diffuse deeper into the tungsten bulk. This could be the reason that some experiment shows that the depths of deuterium accumulation are in the range of several μm [6].

3.1.3. Deuterium stopping time

Fig. 3 shows the average time required for a deuterium atom implanted in the tungsten to come to rest. Higher tungsten temperature slows down the deuterium deceleration process, because the deuterium energy loss from each collision is relatively lower. Higher deuterium energy needs more collisions, thus more time is required for the slowing down process. All the curves are roughly linear beyond the deuterium incident energy of 50 eV.

3.2. Deuterium bubbles formation

To simulate deuterium bubbles formation in tokamak plasma environment, the tungsten sample was repeatedly bombarded by 100 eV deuterium atoms with an incident angle of 25° until the bubble is fully formed. For every 5000 steps, a deuterium atom will be randomly created five lattice parameters (15.825 Å) above the tungsten surface. The initial positions were far enough that when

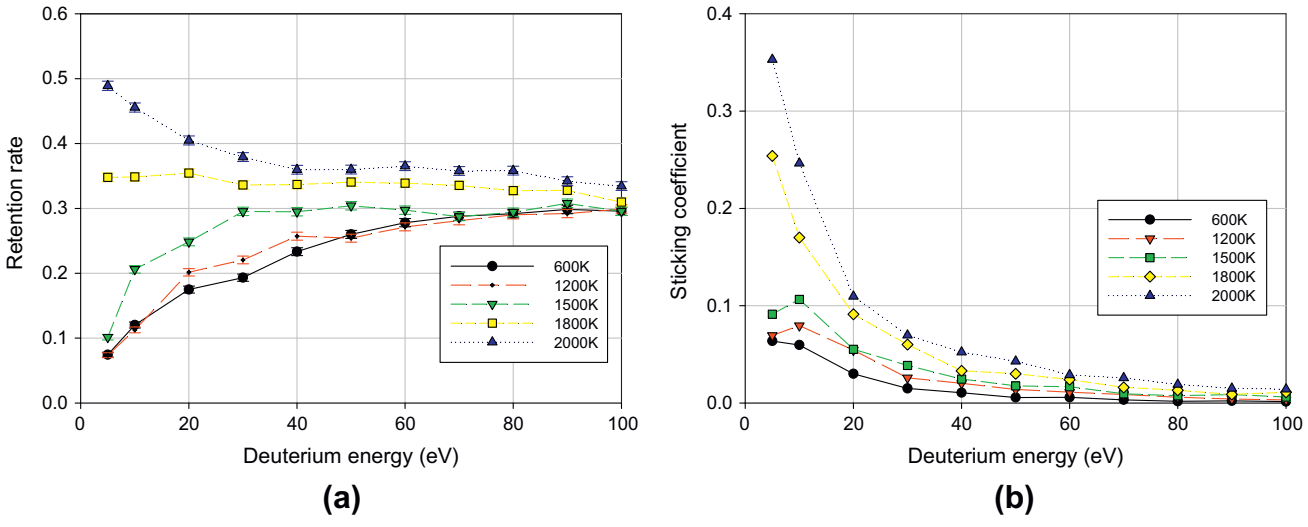

Fig. 1. Deuterium retention rate (a) and sticking coefficient (b) for various tungsten sample temperatures and deuterium energies.

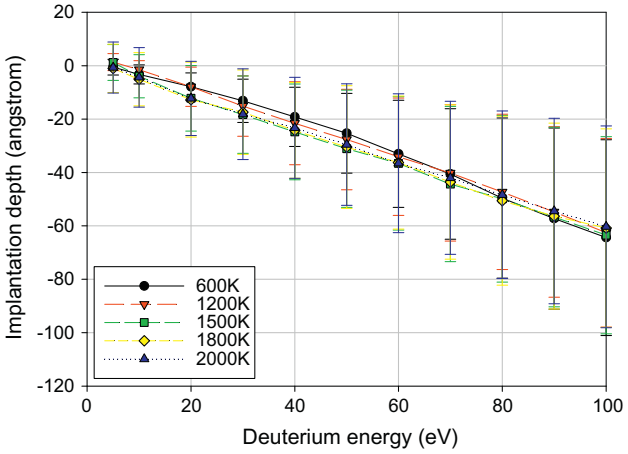

Fig. 2. Average deuterium implantation depth of different tungsten sample temperatures and deuterium energies.

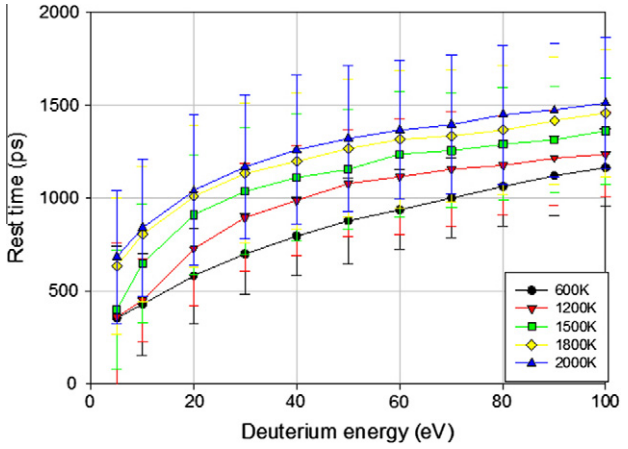

Fig. 3. Average deuterium stopping time for different tungsten temperatures.

the bubble was fully formed and the tungsten swelled toward the z positive direction, the deuterium initial position will still be above the tungsten surface. During the bombardment, the step size was also set to 0.5 fs resulting in an incident flux of $1.0 \times 10^{29}\ m^{-2}\ s^{-1}$. Fig. 4 illustrates the evolution of the deuterium bubble in 600 K tungsten substrate. To enhance the visibility of the bubble outline, only tungsten atoms in the region of 5 Å < y < 13 Å (about 2.5 lattice parameters) are shown in the figure and denoted by the white spheres, while all deuterium atoms are shown and denoted by the red spheres.

For the 600 K simulation, the tungsten lattices gradually became amorphous due to the repeated deuterium irradiation as illustrated in Fig. 4a. Because the incident deuterium energy is well below the physical sputtering threshold energy of 200 eV for deuterium on tungsten [30], and no sputtering was observed in these simulations, the incoming deuterium does not cause either direct displacement or sputtering.

The increase in the local high gas pressure gradually pushes the tungsten atoms aside. The amorphous tungsten occurred in the region of −45 Å < z < −30 Å forms an amorphous sub-layer underneath the crystalline surface layer. This effect and the formation mechanism are very similar to the experiments of nitrogen implantation on stainless steel [31], where amorphous sub-layer formed a few μm from the surface, underneath the crystalline surface layer, due to high stresses introduced by the high density of nitrogen atoms.

Later, a small region containing a visible bubble was formed at about 38 Å below the tungsten surface after 1320 impacts, and it began to trap more deuterium (Fig. 4b). This bubble grew rapidly as shown in Fig. 4c–e. With the development and the growth of the bubble, the bubble cap was finally separated from the sample and blew away (Fig. 4f). In Fig. 4e, prior to the bubble cap separation, the upper portion of the tungsten sample swelled towards the surface about 15 Å to form a surface blister. We have also simulated bubble formation and growth in liquid metals and demonstrated bubbles explosion as they reach the surface [8].

Fig. 5 presents the number of deuterium atoms and deuterium molecules in tungsten substrate as a function of time. The blue line in Fig. 5 shows the number of deuterium atoms trapped in the sample at different times. The deuterium slowly accumulated in the sample with a trapping rate of ~25% that is slightly lower than the calculated temporary retention rate of ~30% shown in Fig. 1 because the deuterium atoms may migrate to tungsten surface and escape from the system. Assuming the D_2 molecular bond length is 0.74 Å, the number of D_2 molecules can be counted and plotted as shown by the red line in Fig. 5. After the bubble is formed (after 1320 D impacts), the D_2 molecule number rapidly increases, because the D atoms have a much higher probability to meet each other and recombine in the bubble region.

The gas pressure in the bubble region can be estimated in the following way. After 1400 deuterium impacts, the gas bubble volume was roughly measured as $7.95 \times 10^{-27}\ m^3$. There were 59 deuterium atoms and seven deuterium molecules in the bubble. The average deuterium temperature in the bubble region was measured as 9839 K. The gas bubble pressure can be roughly estimated using the modified Redlich–Kwong equation-of-state given by:

$$\begin{cases} P = \frac{RT}{V_m - b} - \frac{a}{\sqrt{T} V_m (V_m + b)} \\ a = \frac{0.4275 R^2 T_c^{2.5}}{P_c} \\ b = 0.26 V_c \end{cases} \quad (2)$$

where P is the gas pressure, T is the gas temperature, V_m is the molar volume, a and b are constants, T_c is temperature at the critical point, P_c is pressure at the critical point, and V_c is the critical molar volume.

The calculated gas pressure is about 1.1 GPa. The pressure necessary for the elastic deformation calculated by finite element calculation based on continuum mechanics in the elastic assumption shows that a gas pressure of ~0.1 GPa is sufficient to cause elastic deformation [32]. The calculated bubble pressure is far above the pressure for elastic deformation indicating plastic deformation. The gas bubble pressure is larger than the yield strength (0.5–1 GPa) [32] and in the range of the ultimate strength (1.5 GPa) of W, leading to cause plastic deformation. Therefore, the calculated result indicates that the tungsten sample could significantly suffer large swelling, cracking, and exhibit exfoliation due to the internal high gas pressure.

The same simulation was also performed for 300, 900, and 1200 K tungsten samples. No bubble was found in the 300 K tungsten after 5000 deuterium impacts. Similar vacancies were observed in 900 and 1200 K tungsten substrates after 2339 and 1950 impacts, respectively, and bubbles were formed 34 Å and 87 Å below the surface, respectively. When the bubbles were fully formed, the gas pressure is estimated to be 0.7 and 1.2 GPa, respectively. Tokunaga et al. [33] found surface blister on 343 K single-crystalline tungsten irradiated by 100 eV deuterium using a flux of $10^{22}\ m^{-2}\ s^{-1}$, but not at 383, 623, and 1123 K. Alimov et al. [34] showed that blisters were observed on the surface of single-crystalline tungsten sample with a temperature in the range from 373 to 533 K, when irradiated by the 200 eV deuterium ions with a

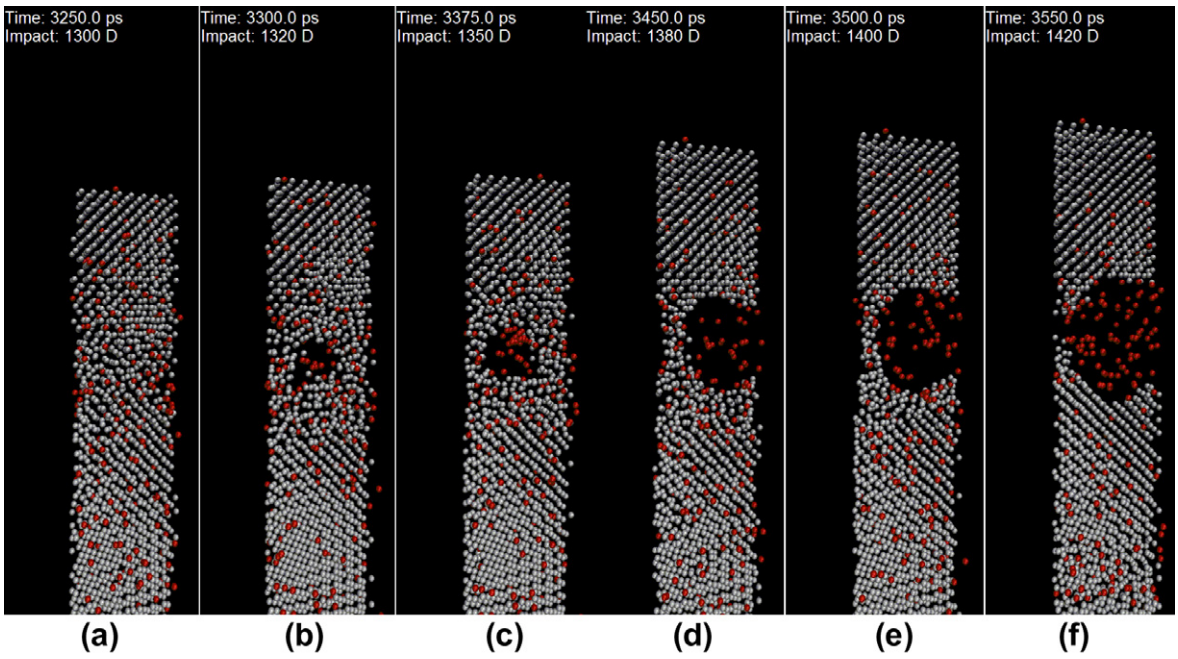

Fig. 4. Snapshots of different phases of the deuterium bubble formation in 600 K tungsten sample bombarded by 100 eV deuterium atoms.

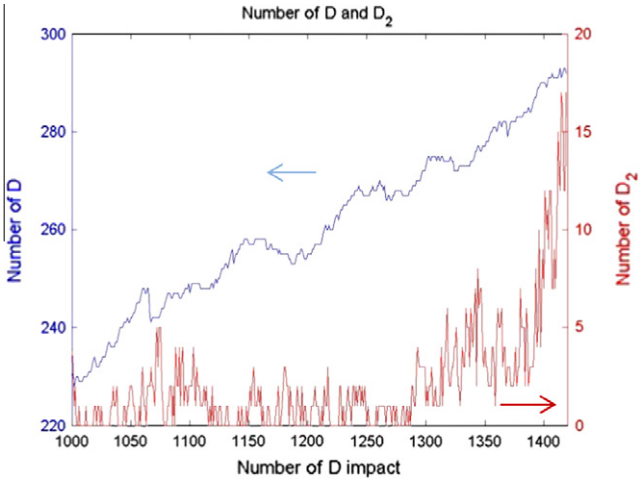

Fig. 5. Number of deuterium atoms and molecules in the 600 K tungsten sample.

flux of 10^{21} m^{-2} s^{-1}, however blisters were not found on the 303 K sample [34]. The high particle flux used in this simulation may account for the difference, since the flux used in this work is several orders of magnitude higher than those experiments.

Recent experiments indicate that the diffusion process may play an important role in the deuterium blister formation on tungsten surface, since cluster of hydrogen and vacancies may diffuse deeply into the bulk and form blisters beyond the range of the implantation depth [34,35]. However, the diffusion process does not play an important role in the MD simulation described above due to the short time scale of the simulation compared to the estimated time scale for the blister formation of seconds to minutes. A review of hydrogen bubbles in metals by Condon and Schober [36] suggested one possible mechanism of void formation. The hydrogen supersaturation can occur as a result of high flux of sudden hydrogen ion implantation. If the hydrogen buildup at the near surface layer has a rate, which is greater than the rate of surface desorption or dissolution into the metal bulk, the hydrogen will nucleate into small bubbles that grows with metal mechanical deformation, yielding blisters. Due to the high flux used in the simulation, the hydrogen has no time to diffuse into the bulk and then accumulates near the surface layer. Therefore, the bubbles were formed several nanometers below the surface instead of the micrometer range. For the 300 K simulation, the trapped deuterium atoms were migrating to deeper tungsten bulk or escaping from the tungsten surface compared to other cases that have higher substrate temperatures. Therefore, deuterium concentration at near surface layer may not reach the required super-saturation state, thus bubbles were not formed after 5000 deuterium impacts in low temperature cases. Bubbles may form after more ion implantation, and/or form deep in the bulk. Due to the required prolonged simulation time, those phenomena are not investigated in this work. In addition, we have performed dynamic Monte Carlo simulation of D diffusion in W and confirmed that is very low. One still needs some diffusion of D to form and reach bubbles and bubble may not be formed at very low temperature since the implanted D will be near frozen in matrix [29].

4. Conclusion

The interaction of deuterium with monocrystalline tungsten was simulated using classical molecular dynamics methods. A Tersoff type interatomic potential was used in LAMMPS code to simulate deuterium bombardment on tungsten as potential plasma facing material in tokamak environment. Tungsten substrate at different temperatures of 600, 1200, 1500, 1800, and 2000 K was bombarded non-accumulatively by deuterium ions with low energies of 5–100 eV and an incident angle of 25° to simulate fusion conditions. The deuterium trapping rate, implantation depth, and stopping time were calculated. For tungsten temperature higher than 1800 K, the trapping rate of the low energy deuterium is higher than the rate of the high-energy deuterium due to the increased surface sticking probability for low energy deuterium. This effect does not influence the higher energy deuterium, since it penetrates deeper into bulk positions. The tungsten temperature does not significantly affect deuterium implantation depth which is proportional to the incident deuterium energy, but affect the deuterium

stopping time. Higher tungsten temperatures slightly slow down the deuterium deceleration process.

Blister formation on tungsten surface due to the deuterium cumulative bombardment was also studied. The 300, 600, 900, and 1200 K tungsten substrates were repeatedly bombarded by 100 eV deuterium using a flux of 1.0×10^{29} m^{-2} s^{-1}. The bombardment lasted till the observation of the fully formed bubble or 5000 deuterium impacts. The simulated deuterium cluster results from the super-saturation of the deuterium at the near surface layer and the subsequent plastic deformation due to the local high gas pressure that exceeds the deformation threshold value. The deuterium gas bubble was observed in the 600, 900, and 1200 K temperature cases, but not for the 300 K case. This result matches previous experiments. A possible explanation of not forming bubble in 300 K case is that the embedded deuterium atoms couldn't move much to locations where bubble nucleation takes place and therefore, super-saturation was not reached at near surface layers up to 5000 impacts used. Further studies are needed to better understand bubble formation, cracking, and bubble explosion during hydrogen isotopes interaction with tungsten as potential plasma facing material.

Acknowledgement

This work is partially supported by the US Department of Energy, Office of Fusion Energy Sciences.

References

[1] J. Roth, E. Tsitrone, A. Loarte, Th. Loarer, G. Counsell, R. Neu, V. Philipps, S. Brezinsek, M. Lehnen, P. Coad, Ch. Grisolia, K. Schmid, K. Krieger, A. Kallenbach, B. Lipschultz, R. Doerner, R. Causey, V. Alimov, W. Shu, O. Ogorodnikova, A. Kirschner, G. Federici, A. Kukushkin, J. Nucl. Mater. 390–391 (2009) 1.
[2] M. Poon, R.G. Macaulay-Newcombe, J.W. Davis, A.A. Haasz, J. Nucl. Mater. 307–311 (2002) 723.
[3] M. Poon, R.G. Macaulay-Newcombe, J.W. Davis, A.A. Haasz, J. Nucl. Mater. 337–339 (2005) 629.
[4] R.E. Nygren, R. Raffray, D. Whyte, M.A. Urickson, M. Baldwin, L.L. Snead, J. Nucl. Mater. 417 (2011) 451.
[5] K.O.E. Henriksson, K. Nordlund, J. Keinonen, Nucl. Instrum. Methods B 244 (2006) 377.
[6] K.O.E. Henriksson, K. Nordlund, J. Keinonen, D. Sundholm, M. Patzschke, Phys. Scripta T108 (2004) 95–98.
[7] K.O.E. Henriksson, K. Nordlund, J. Keinonen, Nucl. Instrum. Method B 244 (2006) 377–391.
[8] Z. Insepov, A. Hassanein, J. Nucl. Mater. 337–339 (2005) 912–916.
[9] Katharina. Vörtler, Kai. Nordlund, J. Phys. Chem. C 114 (2010) 5382–5390.
[10] K. Vörtler, C. Björkas, K. Nordlund, J. Phys.: Condens. Matter 23 (2011) 085002.
[11] Nicola. Gaston, Shaun. Hendy, Catal. Today 146 (2009) 223–229.
[12] P. Träskelin, N. Juslin, P. Erhart, K. Nordlund, Phys. Rev. B 75 (2007) 174113.
[13] Kaoru Ohya, Naohide Mohara, Kensuke Inai, Atsushi Ito, Hiroaki Nakamura, Yoshio Ueda, Tetsuo Tanabe, J. Plasma Fusion Res. Ser. (2010) 497.
[14] Z. Yang, Q. Xu, R. Hong, Q. Li, G. Luo, Fusion Eng. Des. 85 (2010) 1517–1520.
[15] K. Ohya, N. Mohara, K. Inai, A. Ito, H. Nakamura, A. Kirschner, D. Borodin, Fusion Eng. Des. 85 (2010) 1167–1172.
[16] Kaoru Ohya, Kensuke Inai, Yasuyuki Kikuhara, Tomohide Nakano, Jun Kawata, Hayato Kawazome, Yoshio Ueda, Tetsuo Tanabe, J. Plasma Fusion Res. ser. 8 (2009) 419–424.
[17] Xiao.-Chun. Li, F. Gao, Guang-Hong Lu, Nucl. Instrum. Methods 267 (2009) 3197–3199.
[18] K.O.E. Henriksson, K. Nordlund, A. Krasheninnikov, J. Keinonen, Fusion Sci. Technol. 50 (2006) 43–57.
[19] K.O.E. Henriksson, K. Vörtler, S. Dreißigacker, K. Nordlund, J. Keinonen, Surf. Sci. 600 (2006) 3167–3174.
[20] S.J. Plimpton, J. Comp. Phys. 117 (1995) 1. <http://lammps.sandia.gov>.
[21] I.S. Landman, Fusion Eng. Des. 75–79 (2005) 417.
[22] I.S. Landman, H. Wuerz, J. Nucl. Mater. 313–316 (2003) 77.
[23] A.K. Rappié, C.J. Casewit, K.S. Colwell, W.A. Goddard III, W.M. Skiff, J. Am. Chem. Soc. 114 (1992) 10024.
[24] N. Juslin, P. Erhart, P. Träskelin, J. Nord, K.O.E. Henriksson, K. Nordlund, E. Salonen, K. Albe, J. Appl. Phys. 98 (2005) 123520.
[25] X. Li, X. Shu, Y. Liu, F. Gao, G. Lu, J. Nucl. Mater. 408 (2011) 12.
[26] R.J. Kurtz, Highlights of Recent Fusion Materials Tungsten Research, Presented at: MASCO/PFC Joint Session on Tungsten Research, Oak Ridge National Laboratory, Oak Ridge, TN, August 10 2011.
[27] K. Tokunaga, M. Takayama, T. Muroga, N. Yoshida, J. Nucl. Mater. 220–222 (1995) 800–804.
[28] M. Kaufmann, R. Neu, Fusion Eng. Des. 82 (2007) 521.
[29] T. Sizyuk, A. Hassanein, J. Nucl. Mater. 404 (2010) 60–67.
[30] G. Federici et al., Nucl. Fus. 41 (12R) (2001) 1967.
[31] X. Li, Microstructural characterization of nitrogen implanted and plasma nitride austenitic stainless steel, Doctor of Philosophy thesis, Department of materials engineering, University of Wllongong, 1996. <http://ro.uow.edu.au/thesis/1510>.
[32] M. Balden, S. Lindig, A. Manhard, J. You, J. Nucl. Mater. 414 (2011) 69.
[33] K. Tokunaga, M.J. Baldwin, R.P. Doerner, N. Noda, Y. Kubota, N. Yoshida, T. Sogabe, T. Kato, B. Schedler, J. Nucl. Mater. 337–339 (2005) 887–891.
[34] V.Kh. Alimov, J. Roth, R.A. Causey, D.A. Komarov, Ch. Linsmeier, A. Wiltner, F. Kost, S. Lindig, J. Nucl. Mater. 375 (2008) 192–201.
[35] W.M. Shu, A. Kawasuso, T. Yamanishi, J. Nucl. Mater. 386–388 (2009) 356–359.
[36] J.B. Condon, T. Schober, J. Nucl. Mater. 207 (1993) 1–24.